J Appl Physiol 100: 186–193, 2006.
First published September 15, 2005; doi:10.1152/japplphysiol.00424.2005.

Quantitative characterization of airspace enlargement in emphysema

Harikrishnan Parameswaran, Arnab Majumdar, Satoru Ito, Adriano M. Alencar, and Béla Suki
Department of Biomedical Engineering, Boston University, Boston, Massachusetts

Submitted 14 April 2005; accepted in final form 12 September 2005

Parameswaran, Harikrishnan, Arnab Majumdar, Satoru Ito, Adriano M. Alencar, and Bela Suki. Quantitative characterization of airspace enlargement in emphysema. *J Appl Physiol* 100: 186–193, 2006. First published September 15, 2005; doi:10.1152/japplphysiol.00424.2005.—The mean linear intercept (L_m) can be used to estimate the surface area for gas exchange in the lung. However, in recent years, it is most commonly used as an index for characterizing the enlargement of airspaces in emphysema and the associated severity of structural destruction in the lung. Specifically, an increase in L_m is thought to result from an increase in airspace sizes. In this paper, we examined how accurately L_m measures the linear dimensions of airspaces from histological sections and a variety of computer-generated test images. To this end, we developed an automated method for measuring linear intercepts from digitized images of tissue sections and calculate L_m as their mean. We examined how the shape of airspaces and the variability of their sizes influence L_m as well as the distribution of linear intercepts. We found that, for a relatively homogeneous enlargement of airspaces, L_m was a reliable index for detecting emphysema. However, in the presence of spatial heterogeneities with a large variability of airspace sizes, L_m did not significantly increase and sometimes even decreased compared with its value in normal tissue. We also developed an automated method for measuring the area and computed an equivalent diameter of each individual airspace that is independent of shape. Finally, we introduced new indexes based on the moments of diameter that we found to be more reliable than L_m to characterize airspace enlargement in the presence of heterogeneities.

gas exchange

EMPHYSEMA IS DEFINED AS the "abnormal permanent enlargement of the airspaces distal to the terminal bronchioles, accompanied by destruction of their walls and without obvious fibrosis" (1, 33). In recent years, it has become widely accepted to use the mean linear intercept (L_m) (7, 38, 39) to confirm the presence of emphysema in various animal models (20, 23). The likely reason is that L_m is perceived as an index of airspace size (5, 11, 12, 19, 27), although strictly speaking it is a measure of surface area-to-volume ratio (7, 14). During the progression of emphysema, while the surface area decreases, airspace enlargement also occurs. However, being an index of surface area-to-volume ratio, it is not clear whether L_m can be used to characterize airspace enlargement.

Recently, it has been suggested that the destruction of alveolar walls in emphysema necessarily leads to spatially heterogeneous structure (35), with a significantly increased variability of airspace sizes (2, 16, 18, 30). This has important implications for the quantification of airspace enlargement using L_m: airspaces that are abnormally enlarged are often surrounded by many smaller ones. In such cases, L_m may not be sensitive enough to detect enlarged airspaces. Indeed, it has been previously shown that L_m is not adequate to distinguish mild grades of emphysema identifiable by the naked eye (37).

In this paper, we analyzed the suitability of the distribution of linear intercepts (LI), also known as airspace chord lengths (25, 34), and their mean, L_m, as indicators of airspace dimensions. We developed an automated method for measuring the area of individual airspaces from histological sections. We defined an equivalent diameter of an airspace (d) as proportional to the square root of its area, similar to previous definitions in three dimensions (40). We also introduced a family of new indexes based on the moments of d. These new indexes were found to detect the presence of enlarged airspaces in emphysematous tissue sections, even in cases where L_m did not increase or even showed a decrease compared with its value in normal tissue.

METHODS

We analyzed various computer-generated geometric shapes as well as alveolar structures from images of hematoxylin and eosin-stained lung tissue sections fixed in formalin obtained from control and elastase-treated mice (17). First, the original image (Fig. 1*A*) was separated into tissue and airspace. To do this, the original image was thresholded to obtain a binary image, with black representing tissue and white representing airspace (Fig. 1*B*). The threshold level could be selected manually or computed automatically from the original image (26, 41).

Automated measurement of L_m. To estimate L_m, a uniform grid of horizontal and vertical lines was superimposed on the binary image (Fig. 1*B*). The air-tissue interfaces divide each grid line into chords that were either inside an airspace or inside tissue. The length of chords that were inside airspaces were measured and recorded as LI. Airspaces that are only partially in the field of view lead to chords that are terminated on one end by the image boundary. Because the length of such chords are not known, a correction method has to be applied to obtain an unbiased estimate of L_m. In this paper, we used a method due to Oldmixon et al. (25). An alternative approach due to Huang et al. (15) may also be used for this purpose. It should be noted that if the thickness of alveolar walls is assumed to be negligible, the estimate of L_m obtained using the Oldmixon et al. method is identical to that obtained using the traditional approach of counting the number of intersections made by a line with the alveolar walls (7, 25).

Automated measurement of equivalent diameter. To measure airspace area and diameter, the binary image was first segmented into distinct airspaces using the watershed transform (4, 28). The process of segmenting the image can be described briefly as follows. From the binary image, first a distance map was calculated, such that every pixel representing air in the binary image was replaced by the negative of the Euclidean distance between that pixel and the nearest pixel representing tissue. Thus the resulting distance map had basins corresponding to airspaces as illustrated in Fig. 1*C*, where the pixels at the center of the airspace that were farthest from the boundary had the largest negative values (represented by darker shades of gray) and

Address for reprint requests and other correspondence: B. Suki, Dept. of Biomedical Engineering, Boston Univ., 44 Cummington St., Boston, MA 02215 (e-mail: bsuki@bu.edu).

The costs of publication of this article were defrayed in part by the payment of page charges. The article must therefore be hereby marked "*advertisement*" in accordance with 18 U.S.C. Section 1734 solely to indicate this fact.

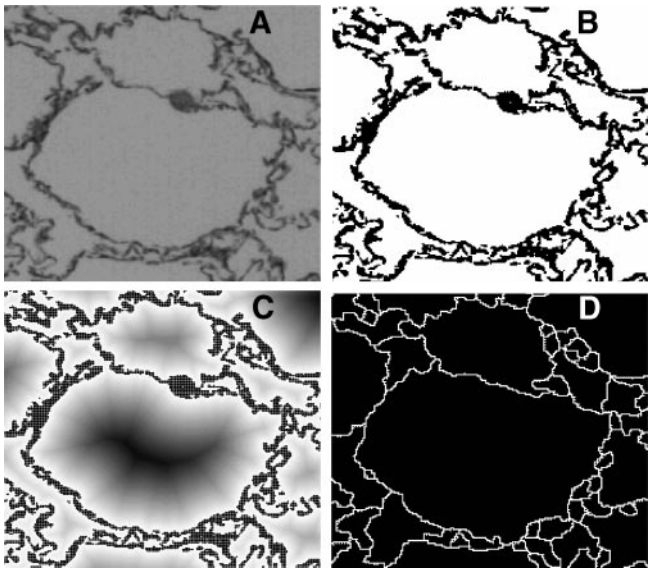

Fig. 1. Illustration of the method of segmentation. *A*: grayscale image. *B*: binary image. *C*: distance map. *D*: segmented image.

those that were closer to the boundary had smaller negative values. Pixels corresponding to tissue in the binary image were assigned a distance of zero.

A regional minimum in the distance map was defined as a connected set of pixels having a constant grayscale value (I_m) and whose external boundary pixels ($\{I_b\}$) all had values higher than I_m. Each regional minimum was characterized by its depth (h) = $\min\{I_b\} - I_m$. To identify a single minimum in each separate airspace, every regional minimum with depth larger than a threshold value was identified with a unique label. The use of a threshold in the labeling process was to avoid the shallow regional minima formed by the irregular shape of the airspace-tissue boundary. Each labeled region was then grown by iteratively increasing the grayscale level in unit steps. Pixels where two different labeled regions met were marked as boundary pixels. The process was stopped when the maximum grayscale level was reached (4). The set of boundary pixels obtained at the end of the watershed transform segments the image into distinctly labeled regions, each representing an airspace (Fig. 1*D*). The area of an airspace (A_i) was then measured by counting the number of pixels inside a labeled region (i) and scaling it to physical dimensions. The corresponding equivalent airspace diameter (d_i) was calculated as:

$$d_i = 2\sqrt{\frac{A_i}{\pi}} \qquad (1)$$

which is equal to the diameter of a circle with area A_i.

Characterizing airspace enlargement using d. To compare normal and emphysematous tissue sections using d, we introduced a family of indexes (D_ν), defined as the ratio of two moments of d

$$D_\nu = \frac{\langle d^{\nu+1}\rangle}{\langle d^{\nu}\rangle} \quad \nu = 0,1,2\ldots \qquad (2)$$

where $\langle \ldots \rangle$ indicates the arithmetic mean.

For $\nu = 0$, $D_0 = \langle d \rangle$ is simply the arithmetic mean of the airspace diameters. For $\nu > 0$, D_ν contains information about the higher order moments of the diameter distribution. For example, D_1 is a function of the mean (μ) and the variance (σ^2) of the diameter distribution. D_2 is a function of μ, σ^2, and the skewness (γ) of the diameter distribution, and so on. In practice, however, the estimation of higher order moments from data can be prone to numerical errors. Hence, we restrict our analysis to $\nu < 3$.

To systematically compare L_m and D_ν, we studied how these indexes characterize heterogeneous and uniform enlargement of a variety of idealized shapes. We also measured L_m and D_ν from digitized images of histological sections and examined their effectiveness in distinguishing normal and emphysematous tissue.

RESULTS

We first focus our analysis on factors that determine the LI distribution and L_m. Specifically, we show that the LI distribution and L_m are dependent on the shape of the airspaces. Next, we analyze the performance of L_m under conditions of increasing variability in the size of airspaces and compare the results with those obtained using D_ν. Finally, we present L_m and D_ν measurements from images of normal and emphysematous lung tissue sections.

Shape dependence of L_m. The shape dependence of L_m is laid out in the Crofton-Cauchy formula (21, 32), which relates L_m to the area (A) and perimeter (P) of a two-dimensional object

$$P = \pi \frac{A}{L_m} \qquad (3)$$

The three dimensional counterpart of *Eq. 3* is given by

$$S = 4\frac{V}{L_m} \qquad (4)$$

where S is the surface area and V is the volume. *Equations 3* and *4* make L_m a useful method for estimating perimeter and surface area of a single object with known area and volume, respectively. To verify that *Eq. 3* holds for airspaces in histological sections of the lung, we randomly selected airspaces from segmented images of lung tissue and computed L_m, perimeter, and area of the selected airspaces. When L_m was plotted against the ratio of area to perimeter of the airspaces (Fig. 2*A*), we found a strong linear relationship with a slope close to π (3.09 $\pm$ 0.01) and an intercept close to zero (-3.66 ± 0.41 μm). For a collection of airspaces (Fig. 2*B*), L_m was found to be proportional to the ratio of total area to the total perimeter, with a slope of 2.97 $\pm$ 0.01 and an intercept of -2.9 ± 0.5 μm.

When L_m is used as a measure of the linear dimensions of airspaces, using *Eq. 3*, it can be shown that L_m depends not only on the dimensions of the object but also on its shape. Indeed, *Eq. 3* implies that

$$L_m = \pi\frac{\sqrt{A}}{P}\sqrt{A} = \zeta\sqrt{A}$$

where ζ is a dimensionless quantity that depends only on shape.

To study how the shape influences the LI distribution, a simple test image containing a collection of randomly oriented identical ellipses was created. The shape of these ellipses was controlled by changing their eccentricity (ϵ), defined as the ratio of the distance between the two focii of the ellipse to the length of its major axis. The first test image contained circles, which can be considered as ellipses with $\epsilon = 0$ (Fig. 3*A*). By increasing ϵ, the circles were transformed into randomly oriented ellipses having the same area (Fig. 3*B*). The equivalent diameter in both cases was 65 pixels, but L_m changed from 51 pixels ($\sigma = 14$) to 42 pixels ($\sigma = 18$). The corresponding LI

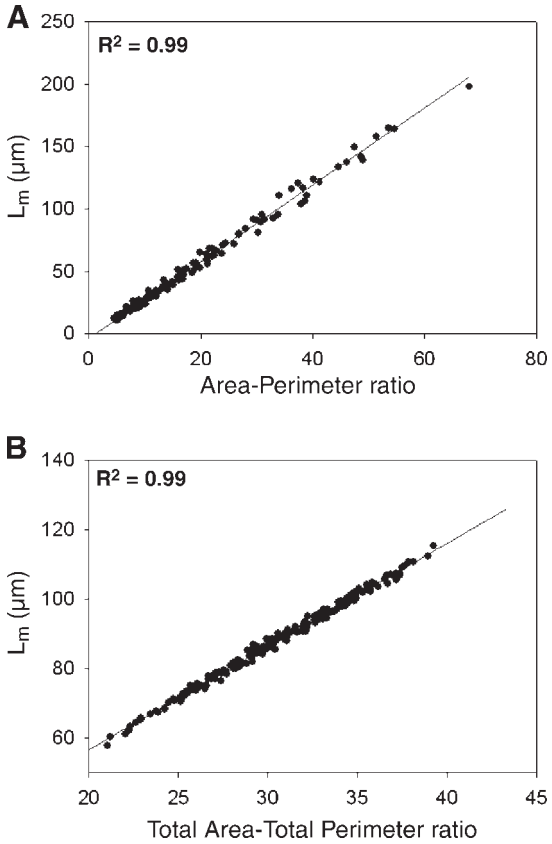

Fig. 2. Dependence of mean linear intercept (L_m) on the area-to-perimeter ratio. *A*: each dot corresponds to a single airspace that was randomly selected from lung tissue sections. *B*: each dot corresponds to a collection of 30 airspaces that were randomly selected from lung tissue sections. Solid lines show linear regression fit to the data.

distributions are shown in Fig. 3*C*, and their derivation is given in APPENDIX A. This clearly shows that the LI distribution as well as its mean and variance are sensitive to changes in shape. Another interesting observation here was the large spread of the LI distribution. L_m in Fig. 3*B* had a standard deviation that was 42% of the mean, although all the objects had identical dimensions. The high variability was entirely due to the shape of the objects.

These results indicate that the use of L_m to characterize changes in dimensions of airspaces under various experimental conditions is only accurate when the shape of the airspaces does not change appreciably. Furthermore, even the LI distribution may not be used to calculate indexes of heterogeneity like the coefficient of variation (CV), defined as σ/μ, because of its dependency on the shape of individual airspaces in the section. In contrast, the distribution of d is by definition (*Eq. 1*) shape independent.

Characterizing heterogeneous enlargement of airspaces. We examined whether the mean airspace diameter (D_0) can detect airspace enlargement. An arithmetic mean gives equal weight to all the airspaces in the tissue section. Consequently, if there were many small airspaces accompanied by a few enlarged ones, then D_0 would have a value close to the dimensions of the smaller airspaces simply because there are a large number of them compared with the enlarged airspaces. One possible solution to this problem is to use a weighted mean measure, like D_v, where enlarged airspaces are weighted more than normal airspaces.

D_v can be expressed as functions of the central moments of airspace diameters. Specifically, D_1 is a function of the mean (μ) and variance (σ^2) of airspace diameters as:

$$D_1 = \frac{\langle d^2 \rangle}{\langle d \rangle} = \mu\left(1 + \frac{\sigma^2}{\mu^2}\right) \quad (5)$$

and D_2 is a function of μ, σ^2, and skewness (γ) of the diameter distribution

$$D_2 = \frac{\langle d^3 \rangle}{\langle d^2 \rangle} = \mu\left[1 + \frac{\sigma^2}{\mu^2 + \sigma^2}\left(2 + \frac{\sigma\gamma}{\mu}\right)\right] \quad (6)$$

Equations 5 and *6* are derived in APPENDIX B. D_v can therefore be thought of as a generalized measure of the airspace dimensions, which, unlike L_m, is independent of shape.

To analyze the effects of variability in airspace sizes on L_m and D_v, we considered images consisting of a circle of radius R surrounded by a symmetric packing of circles, each having a radius r. Starting from a configuration where $R = r$ (Fig. 4*A*), the ratio R/r was increased in steps, such that the total area of the circles was unity. The number of circles of radius r was chosen such that they provided a close packing around the circumference of the central circle (Fig. 4, *A* and *B*). For each step, we computed L_m, D_0, and D_2 for the corresponding image. In this case, since all the objects under consideration

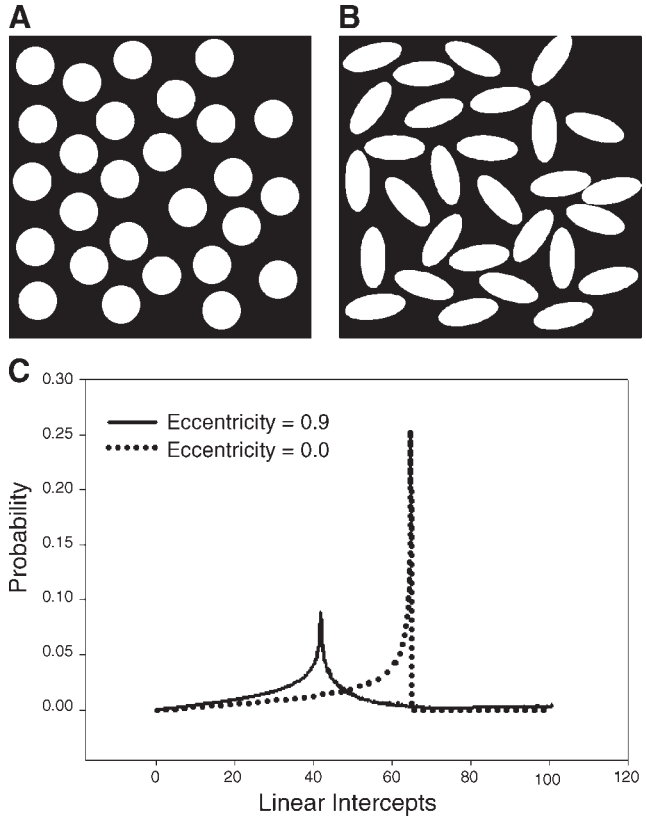

Fig. 3. Illustration of the shape dependence of linear intercept (LI) distribution. *A*: circles or ellipses with zero eccentricity and mean diameter of 65 pixels. *B*: ellipses with the same area as *A* but with eccentricity of 0.9. *C*: LI distributions from *A* and *B* show a large spread even though there is no change in area of the objects.

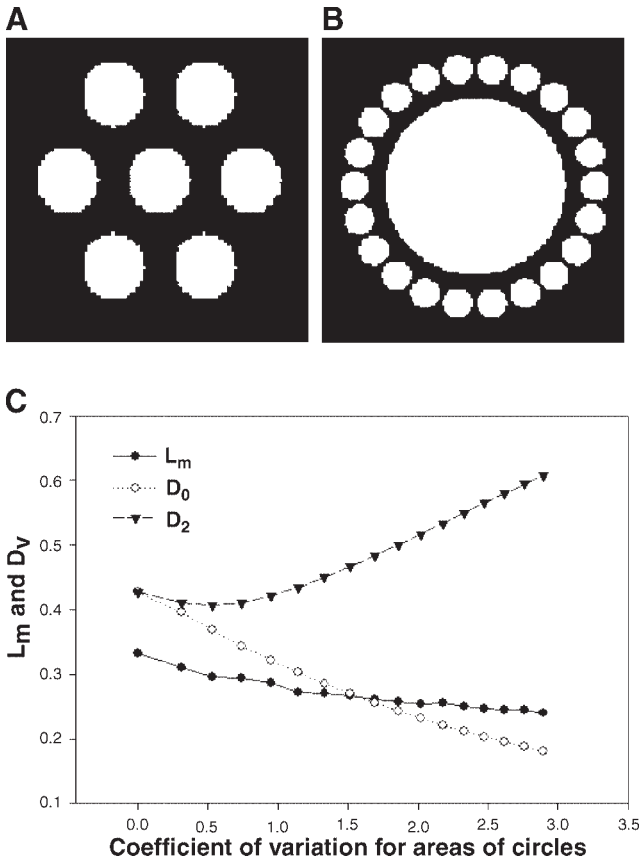

Fig. 4. *A*: test image including circles with no variability in their size. The radius of the central circle, *R*, is the same as the radii of the circles surrounding it, *r*, i.e., $R = r$. *B*: test image including circles with significant variability in size. The central circle has a radius $R = 6r$. *C*: L_m, mean airspace diameter (D_0), and D_2 as functions of the coefficient of variation of circle areas.

were of the same shape, $L_m \propto D_1$ (see DISCUSSION), and hence we plotted only L_m in Fig. 4*C*.

The variability in the sizes of the objects can be characterized by the CV of the areas. As the CV increased, the dimensions of the surrounding circles, which constitute the majority of objects, decreased. Consequently, both L_m (● in Fig. 4*C*) and D_0 (○ in Fig. 4C) decreased. However, the enlargement of the central circle also influences σ^2 and γ, both of which increased. Consequently, D_2 (▼ in Fig. 4*C*) remained sensitive to the enlargement of the central circle and increased with CV.

Analysis of tissue samples. Figure 5 shows three typical images: a normal tissue section, an emphysematous tissue section with relatively homogeneous enlargement of airspaces, and an emphysematous tissue section showing spatially heterogenous enlargement with a large variability in airspace sizes. To study the effectiveness of the different indexes in distinguishing normal and emphysematous tissue samples, L_m, D_1, and D_2 were calculated from 29 images of normal tissue sections and 41 images of emphysematous tissue sections. The indexes D_1 and D_2 were plotted against L_m (Fig. 6). For those sections, which exhibited a reasonably homogenous enlargement of airspaces (Fig. 5*B*), L_m was able to distinguish between normal and emphysematous sections. However, for sections that had a more heterogenous appearance (Fig. 5*C*), L_m even decreased compared with the normal sample (Fig. 5*A*). The overlap between normal and emphysematous samples on the L_m axis (Fig. 6) illustrates the inability of L_m to distinguish between normal and emphysematous tissue. On the D_1 and D_2 axes, however, normal and emphysematous samples were better separated, clearly indicating that these indexes are sensitive to abnormal enlargement of airspaces even in the presence of heterogeneity.

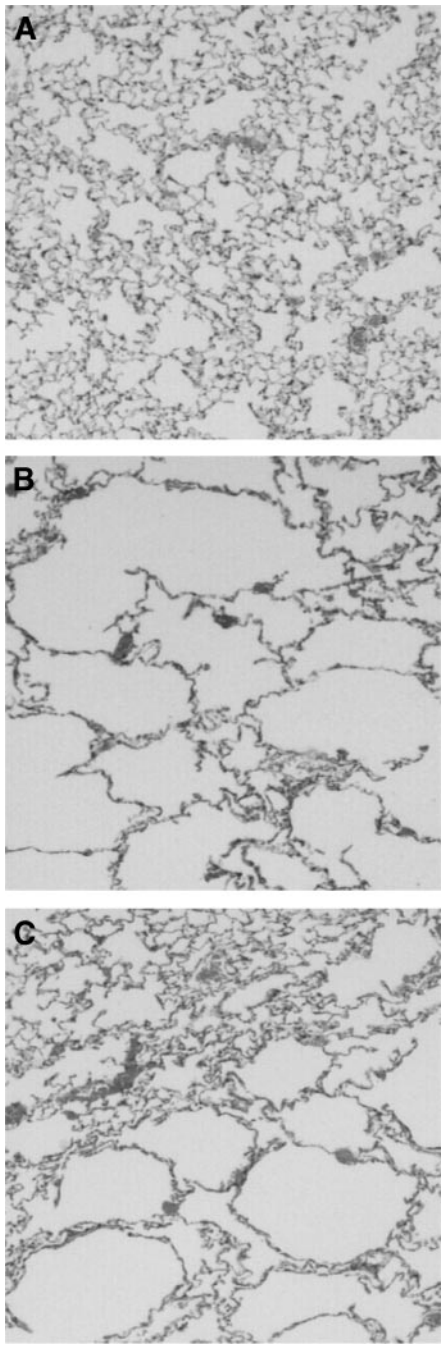

Fig. 5. Examples of hematoxylin and eosin-stained images of tissue samples corresponding to normal lung tissue with $L_m = 94$ μm, $D_1 = 101$ μm, and $D_2 = 126$ μm (*A*), emphysematous tissue with a relatively homogeneous spatial distribution of airspaces with $L_m = 146$ μm, $D_1 = 221$ μm, and $D_2 = 326$ μm (*B*), and heterogeneous spatial distribution of airspaces with $L_m = 84$ μm, $D_1 = 141$ μm, and $D_2 = 239$ μm (*C*).

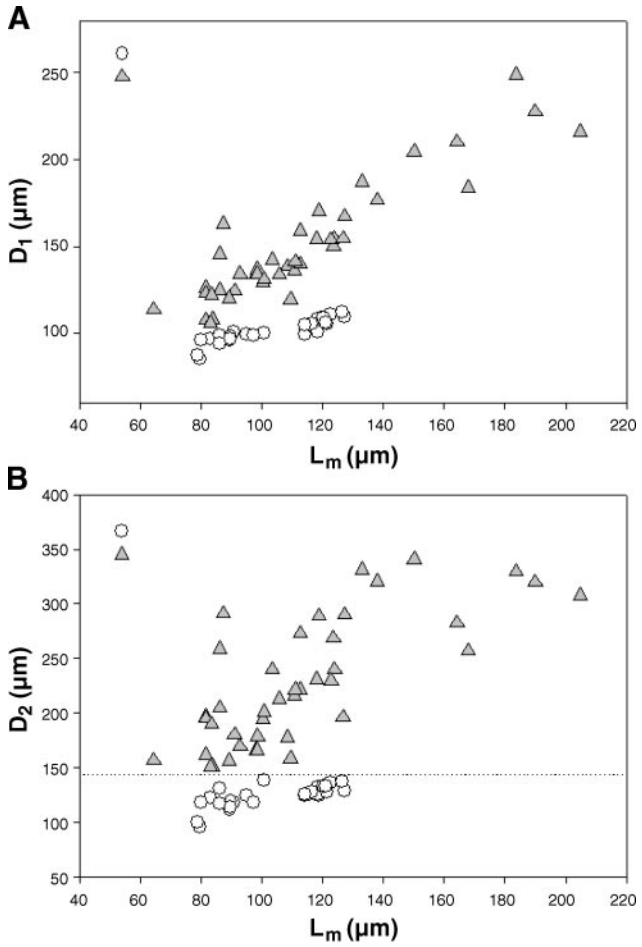

Fig. 6. L_m, D_1, and D_2 measurements from tissue samples. *A*: D_1 plotted against L_m. *B*: D_2 plotted against L_m. The overlap between normal and emphysematous samples on the L_m axis illustrates the inability of L_m to distinguish between normal and heterogenous samples of emphysematous tissue. The samples, however, appear better separated on the D_1 axis and completely separated on the D_2 axis (dotted line).

DISCUSSION

Pulmonary emphysema is a progressive disease characterized by tissue destruction and enlargement of distal airspaces (1, 33). Various methods including L_m (38, 7, 39), destructive index (31), and airspace surface area per unit volume (9) have been used to quantitatively estimate the extent of emphysema from lung tissue sections. Despite its original definition as an index of the ratio of lung volume to surface area (7), L_m has come to be the most widely used measure of airspace enlargement in the parenchyma (5, 19, 27). In this paper, our aim was to examine L_m as a measure of average airspace size. Additionally, we compared L_m to D_v, an index based solely on the equivalent diameters of airspaces, and assessed their effectiveness in identifying emphysema in the presence of a large variability in airspace sizes.

To achieve these goals, we used image-processing algorithms to measure LI and equivalent diameters of airspaces from digitized images of lung tissue. First, we separated the images into regions corresponding to air and tissue using a threshold that was either selected manually or computed from the image itself (26). For images with a high contrast between the air and tissue regions, the automatically selected threshold was reliable and closely matched those chosen manually. We note, however, that for low-contrast images without a sharp air-tissue boundary, the choice of threshold could have a significant effect on the resulting measurements. Next, we measured LI as the chord lengths contained within the airspaces and bounded either by tissue or the image boundary. We computed L_m using a method described by Oldmixon et al. (25) that corrects for the boundary effects. We note that, without this correction, L_m was underestimated by ~15% on average. To measure airspace diameters, we segmented the image into separate airspaces using the watershed transform (28). This technique, however, introduces a second threshold that controls the degree of segmentation. Setting this threshold too low would result in an oversegmented output, and setting it too high would result in the removal of small airspaces. In this paper, this threshold was set by visually comparing the result of the segmentation procedure to the original image. Additionally, this method is not able to automatically identify large airways and unfilled blood vessels, which were excluded manually.

Using this automated image-processing technique, one can make unbiased measurement of the LI directly from stained images of lung tissue. Thus it is possible to characterize parenchymal structure using the full distribution of the chord lengths of alveolar sizes or linear intercept lengths rather than just L_m. Our results, however, indicate that the distribution of LI itself is also sensitive to the shape of individual airspaces. Therefore, the distribution of LI is not very reliable for studying the changes in variability and other higher order moments of airspace dimensions that characterize the heterogenous nature of emphysematous tissue structure.

Apart from the enlargement of airspaces, another important structural change observed in emphysema is the loss of internal surface area or air-tissue interface. Being a function of shape, L_m is also sensitive to changes in surface area. Previous studies (7, 21) have shown that L_m for a three-dimensional object is proportional to the ratio of volume and surface area, which in two dimensions reduces to the ratio of area and perimeter (Fig. 2). Therefore, at a fixed lung volume, L_m is inversely proportional to the internal surface area of the lung. Thurlbeck et. al (37) made extensive internal surface area measurements in the human lung and observed that, in centrilobular emphysema and also in cases of "mild" emphysema, the internal surface area did not significantly decrease below the range found in normal lungs. In all cases studied, however, subjective visual assessment always identified the tissue samples as emphysematous. This finding suggests that the presence of a few abnormally enlarged airspaces among many normal ones might be a more reliable morphological indicator of emphysema than the total change in internal surface area and hence L_m. It has also been recently reported that, in an elastase-induced mouse model of mild emphysema, both the mean size of the airspaces and their CV significantly increased compared with those observed in control lungs (16). Thus a poor correlation between L_m and various measures of lung function (27) may be a consequence of the fact that L_m does not take into account the large variability of airspace sizes in tissue sections. In certain experimental conditions, this may also result in the identification of the wrong mechanism or missing the right mechanism.

Alveolar diameters, unlike the LI, depend only on size, and therefore they can be used to calculate indexes of airspace enlargement like weighted mean diameters. The use of a

weighted mean to characterize abnormal enlargement of airspaces in emphysema is not new. In fact, L_m is itself a weighted mean measure similar to D_1

$$L_m = k\frac{\langle A\rangle}{\langle P\rangle} \propto \frac{\langle d^2\rangle}{\langle (d/\zeta)\rangle} \quad (7)$$

where k is the constant of proportionality from Fig. 2*B*. Thus, although L_m is a weighted mean measure of airspace dimensions, the weight of each airspace depends on its shape due to the shape factor ζ. The indexes D_v also have simple physical interpretations. For example, D_2 can be expressed as

$$D_2 = \frac{\langle d^3\rangle}{\langle d^2\rangle} = \sum_i \left(\frac{A_i}{\sum_j A_j}\right) d_i \quad (8)$$

Therefore, D_2 is a weighted mean measure where every airspace is weighted by the fraction of the total area occupied by it. In a homogeneous and narrow distribution of alveolar sizes, as observed in normal lung tissue samples, the area weighted mean is very close to the arithmetic mean since the fractional area occupied by airspaces is nearly constant. When the distribution of airspace sizes becomes wider with abnormally large airspaces surrounded by many smaller ones, the large airspaces will be weighted significantly more in the calculation of D_2 than in the calculation of L_m since they occupy a higher fraction of the total area than the smaller airspaces. This makes D_2 more sensitive to the presence of enlarged airspaces in a tissue section than L_m or D_0 (Fig. 6).

Computed tomography (CT) provides physicians with a noninvasive tool for assessing alterations in lung structure induced by various disease processes. Many studies have been undertaken to detect and quantify pulmonary emphysema using CT (3, 8, 10, 13). Low attenuation areas (LAA) on CT scans have been shown to represent emphysematous changes in the lungs of patients (3, 24). It has been reported that the cumulative distribution of LAA cluster sizes (A) follows a power law $P(A) \propto A^{-\alpha}$ (22). The exponent α was found to be sensitive to small changes in structure in early emphysema (6, 22). When the LAA cluster sizes follow a power law distribution, it can be shown that D_2 of the LAA clusters is a function of the power law exponent. This suggests that the area of LAA clusters in a CT image could be used to calculate an area-weighted mean diameter value similar to D_2 measured from tissue sections. Thus our new index D_2 may prove useful to characterize the progression of emphysema from macroscopic CT images as well. Nevertheless, the relation between D_2 of LAA, which indicates changes in structure at the scale of a CT voxel, and D_2 from histological sections, which measures changes at the scale of individual alveoli, needs further investigation.

In conclusion, L_m that is currently the most widely accepted index for detecting and quantifying abnormally enlarged airspaces in emphysema is not reliable, especially in the presence of spatially heterogeneous tissue destruction. The weighted mean diameter on the other hand is a robust measure of size and is sensitive to airspace enlargement, even in the presence of heterogeneities. Finally, since emphysema is currently defined as an abnormal increase in airspace dimensions, our findings may have implications for the very definition and the quantitative characterization of the progression of emphysema.

APPENDIX A

Probability Density Function of LI

In this appendix, we derive the probability density function of LI for circles and ellipses. First, we consider a circle of diameter D with intercepts of length λ, where $\lambda \leq D$. Because a circle possesses rotational symmetry, it is sufficient to consider only horizontal intercepts to obtain the probability density function $\Pi(\lambda)$ of intercept lengths. In addition, due to the symmetry between the upper and lower halves of the circle, we calculate the intercepts only in the upper half. The horizontal intercepts are evenly spaced with a density of ρ intercepts per unit length, such that the total number of intercepts ν is given by

$$\nu = \int_0^{D/2} dh\rho = \frac{D}{2}\rho \quad (A1)$$

Figure 7*A* shows that, at a distance h from the center, the intercept length λ satisfies

$$\left(\frac{\lambda}{2}\right)^2 + h^2 = \left(\frac{D}{2}\right)^2 \quad (A2)$$

Thus the lengths of the intercepts λ can be written as a function of h as

$$\lambda(h) = \sqrt{D^2 - 4h^2} \quad (A3)$$

The probability density function $\Pi(\lambda)$ of the intercept length λ is defined as

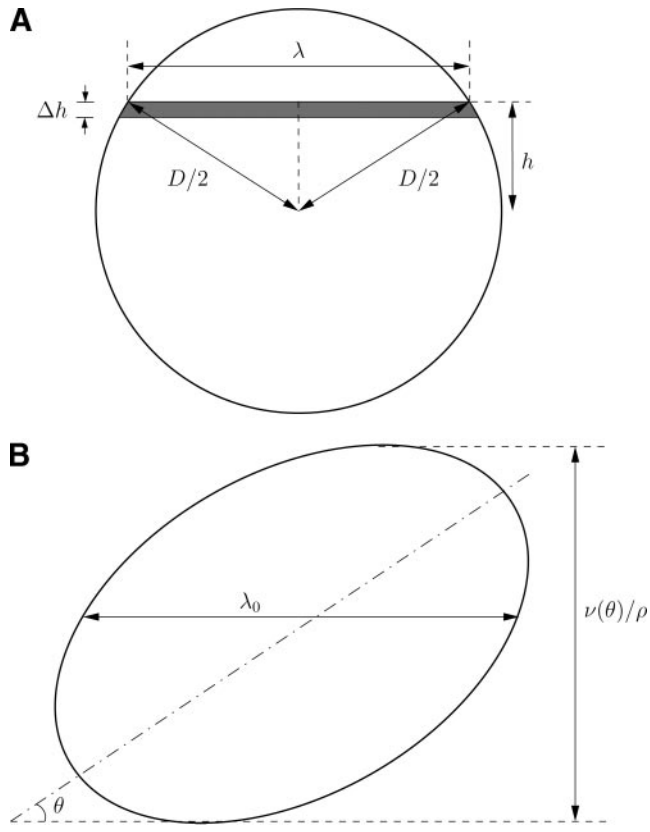

Fig. 7. Illustrations of horizontal intercepts of length λ at distances between h and h-Δh from the center of a circle with diameter D (*A*) and maximum length of the horizontal intercept λ_0 and maximum height of an ellipse at angle θ (*B*).

$$\Pi(\lambda)\Delta\lambda \equiv P[\lambda \le \tilde{\lambda} \le \lambda + \Delta\lambda] \quad (A4)$$

which is the probability of finding an intercept with length $\tilde{\lambda}$ between λ and $\lambda + \Delta\lambda$. Using *Eq. A3*, these intercepts can be found between h and $h - \Delta h$ in the upper semicircle, which satisfies the relations

$$\lambda = \sqrt{D^2 - 4h^2} \quad (A5a)$$

$$\lambda + \Delta\lambda = \sqrt{D^2 - 4(h - \Delta h)^2} \quad (A5b)$$

where $0 < h \le D/2$. Thus the probability density function $\pi(\lambda)$ can be written as

$$\Pi(\lambda)\Delta\lambda = P[h \le \tilde{h} \le h - \Delta h] \quad (A6)$$

$$= \frac{\rho\Delta h}{\nu} \quad (A7)$$

$$= \frac{2\Delta h}{D} \quad (A8)$$

where the last step is obtained by using *Eq. A1*. *Equations A5* can now be used to express Δh in terms of $\Delta\lambda$

$$\Delta h = \frac{\lambda\Delta\lambda}{2\sqrt{D^2 - \lambda^2}} \quad (A9)$$

and thus

$$\Pi(\lambda) = \frac{\lambda}{D\sqrt{D^2 - \lambda^2}} \quad (A10)$$

L_m can then be calculated as

$$L_m = \langle\lambda\rangle = \int_0^D d\lambda\lambda\pi(\lambda) \quad (A11)$$

$$= \frac{\pi}{4} D \approx 0.785D \quad (A12)$$

and the variance of LI is given by

$$\sigma^2(\lambda) = \langle\lambda^2\rangle - \langle\lambda\rangle^2 \quad (A13)$$

$$= \left(\frac{2}{3} - \frac{\pi^2}{16}\right) D^2 \approx (0.223D)^2 \quad (A14)$$

For an ellipse with major axis $2a$ and minor axis $2b$, the calculation of $\pi(\lambda)$ is complicated by the lack of rotational symmetry. We first find the conditional probability density function of horizontal intercept lengths for an ellipse with a particular tilt θ, which can be derived similar to that for a circle, and thus

$$\Pi(\lambda|\theta) = \frac{1}{\lambda_0}\left[\frac{\lambda}{\sqrt{\lambda_0^2 - \lambda^2}}\right] \quad (A15)$$

where λ_0 is the maximum length of a horizontal intercept, given by

$$\lambda_0 = D\frac{(1 - \varepsilon^2)^{1/4}}{\sqrt{1 - \varepsilon^2\cos^2\theta}} \quad (A16)$$

where ε is the eccentricity of the ellipse and $D = 2\sqrt{ab}$ is its equivalent diameter. We note that the total number of lines intersecting a tilted ellipse depends on the angle θ, and is given by

$$\nu(\theta) = \rho\frac{\sqrt{1 - \varepsilon^2\cos^2\theta}}{(1 - \varepsilon^2)^{1/4}} \quad (A17)$$

where ρ is the density of intercepts. Figure 7*B* illustrates λ_0 and $\nu(\theta)$. The probability density function of LI is thus given by

$$\Pi(\lambda) = \frac{1}{\int_0^{\pi/2} d\theta\nu(\theta)} \int_0^{\pi/2} d\theta\nu(\theta)\Pi(\lambda|\theta) \quad (A18)$$

which can be calculated numerically. L_m and the variance of intercept lengths for an ellipse can, however, be calculated exactly as

$$L_m = \frac{\pi^2}{8}\left[\frac{(1 - \varepsilon^2)^{1/4}}{E(\varepsilon^2)}\right] D \quad (A19)$$

$$\sigma_\lambda^2 = \frac{\sqrt{1 - \varepsilon^2}}{E^2(\varepsilon^2)}\left[\frac{2}{3} K(\varepsilon^2)E(\varepsilon^2) - \frac{\pi^2}{64}\right] D^2 \quad (A20)$$

where $K(\ldots)$ and $E(\ldots)$ are the complete elliptic integrals of the first and second kind, respectively. When $D = 65$ pixels for circles with $\varepsilon = 0$, $L_m = 51.0$ pixels with a standard deviation of intercept lengths $\sigma_\lambda = 14.5$ pixels, and for ellipses with $\varepsilon = 0.9$, $L_m = 45.2$ pixels with $\sigma_\lambda = 18.7$ pixels. These values closely match the numerical measurements from Fig. 3.

APPENDIX B

Relating D_ν to the Diameter Distribution

Let μ be the arithmetic mean of the diameter distribution. The equivalent diameter of any airspace in the tissue section can be expressed as $d_i = \mu + \delta_i$. By definition, $\langle\delta\rangle = 0$ and $\langle\delta^2\rangle = \sigma^2$, the standard deviation of airspace diameters. The nth moment of d_i can be calculated as

$$\langle d^n\rangle = \left\langle \sum_{m=0}^{n} \binom{n}{m} \mu^m \delta^{n-m} \right\rangle = \sum_{m=0}^{n} \binom{n}{m} \mu^m \langle\delta^{n-m}\rangle \quad (B1)$$

Using *Eq. B1*, we can relate D_ν to $\nu + 1$ and lower order moments of the diameter distribution. Specifically, for $\nu = 1, 2$

$$D_1 = \frac{\langle d^2\rangle}{\langle d\rangle} = \frac{\langle\delta^2\rangle + 2\mu\langle\delta\rangle + \mu^2}{\mu} = \mu\left(1 + \frac{\sigma^2}{\mu^2}\right)$$

$$D_2 = \frac{\langle d^3\rangle}{\langle d^2\rangle} = \frac{\langle\delta^3\rangle + 3\mu\langle\delta^2\rangle + 3\mu^2\langle\delta\rangle + \mu^3}{\langle\delta^2\rangle + 2\mu\langle\delta\rangle + \mu^2} = \mu\left[1 + \frac{\sigma^2}{\mu^2 + \sigma^2}\left(2 + \frac{\sigma\gamma}{\mu}\right)\right]$$

where $\gamma = \langle\delta^3\rangle/\sigma^3$ is the skewness of the diameter distribution.

REFERENCES

1. **American Thoracic Society.** Definitions, epidemiology, pathophysiology, diagnosis, and staging. *Am J Respir Crit Care Med* 152: S78–S121, 1995.
2. **Baldi S, Miniati M, Bellina C, Battolla L, Catapano G, Begliomini E, Giustini D, and Giuntini C.** Relationship between extent of pulmonary emphysema by high-resolution computed tomography and lung elastic recoil in patients with chronic obstructive pulmonary disease. *Am J Respir Crit Care Med* 164: 585–589, 2001.
3. **Bergin C, Muller N, Nichols DM, Lillington G, Hogg JC, Mullen B, Grymaloski MR, Osborne S, and Pare PD.** The diagnosis of emphysema. A computed tomographic-pathologic correlation. *Am Rev Respir Dis* 133: 541–546, 1986.
4. **Beucher S and Meyer F.** The morphological approach to segmentation: the watershed transform. In: *Mathematical Morphology in Image Processing*. New York: Dekker, 1993, p. 433–481.
5. **Churg A, Wang RD, Tai H, Wang X, Xie C, and Wright JL.** Tumor necrosis factor-α drives 70% of cigarette smoke-induced emphysema in the mouse. *Am J Respir Crit Care Med* 170: 492–498, 2004.
6. **Coxson HO, Whittall KP, Nakano Y, Rogers RM, Sciurba FC, Keenan RJ, and Hogg JC.** Selection of patients for lung volume reduc-

tion surgery using a power law analysis of the computed tomographic scan. *Thorax* 58: 510–514, 2003.
7. **Dunnill M.** Quantitative methods in the study of pulmonary pathology. *Thorax* 17: 320–328, 1962.
8. **Gevenois P, de Maertelaer V, De Vuyst P, Zanen J, and Yernault J.** Comparison of computed density and macroscopic morphometry in pulmonary emphysema. *Am J Respir Crit Care Med* 152: 653–657, 1995.
9. **Gillooly M, Lamb D, and Farrow AS.** New automated technique for assessing emphysema on histological sections. *J Clin Pathol* 44: 1007–1011, 1991.
10. **Goddard PR, Nicholson EM, Laszlo G, and Watt I.** Computed tomography in pulmonary emphysema. *Clin Radiol* 4: 379–387, 1982.
11. **Guerassimov A, Hoshino Y, Takubo Y, Turcotte A, Yamamoto M, Ghezzo H, Triantafillopoulos A, Whittaker K, Hoidal JR, and Cosio MG.** The development of emphysema in cigarette smoke-exposed mice is strain dependent. *Am J Respir Crit Care Med* 170: 974–980, 2004.
12. **Hawgood S, Ochs M, Jung A, Akiyama J, Allen L, Brown C, Edmondson J, Levitt S, Carlson E, Gillespie AM, Villar A, Epstein CJ, and Poulain FR.** Sequential targeted deficiency of SP-A and -D leads to progressive alveolar lipoproteinosis and emphysema. *Am J Physiol Lung Cell Mol Physiol* 283: L1002–L1010, 2002.
13. **Hayhurst MD, MacNee W, Flenley DC, Wright D, McLean A, Lamb D, Wightman AJ, and Best J.** Diagnosis of pulmonary emphysema by computerised tomography. *Lancet* 2: 320–322, 1984.
14. **Heemskerk-Gerritsen BA, Dijkman JH, and Ten Have-Opbroek AA.** Stereological methods: a new approach in the assessment of pulmonary emphysema. *Microsc Res Tech* 34: 556–562, 1996.
15. **Huang YL and Mitzner W.** Distribution analysis of alveolar size by digital imaging. *J Comp Assist Microscopy* 1: 397–409, 1989.
16. **Ito S, Ingenito EP, Arold SP, Parameswaran H, Tgavalekos NT, Lutchen KR, and Suki B.** Tissue heterogeneity in the mouse lung: effects of elastase treatment. *J Appl Physiol* 97: 204–212, 2004.
17. **Ito S, Ingenito E, Brewer KK, Black L, Parameswaran H, Lutchen KR, and Suki B.** Mechanics, nonlinearity, and failure strength of lung tissue in a mouse model of emphysema: possible role of collagen remodeling. *J Appl Physiol* 98: 503–511, 2005.
18. **Kononov S, Brewer KK, Sakai H, Cavalcante FS, Sabayanagam CR, Ingenito EP, and Suki B.** Roles of mechanical forces and collagen failure in the development of elastase-induced emphysema. *Am J Respir Crit Care Med* 164: 1920–1926, 2001.
19. **Lucey EC, Goldstein RH, Breuer R, Rexer BN, Ong DE, and Snider GL.** Retinoic acid does not affect alveolar septation in adult FVB mice with elastase-induced emphysema. *Respiration* 70: 200–205, 2003.
20. **Martorana PA, Beume R, Lucattelli M, Wollin L, and Lungarella G.** Roflumilast fully prevents emphysema in mice chronically exposed to cigarette smoke. *Am J Respir Crit Care Med* 172: 848–853, 2005. First published June 16, 2005; 10.1164/rccm.200411–1549OC.
21. **Mazzolo A, Roesslinger B, and Gille W.** Properties of chord length distributions of nonconvex bodies. *J Mathematical Physics* 44: 6195–6208, 2003.
22. **Mishima M, Hirai T, Itoh H, Nakano Y, Sakai H, Muro S, Nishimura K, Oku Y, Chin K, Ohi M, Nakamura T, Bates JH, Alencar AM, and Suki B.** Complexity of terminal airspace geometry assessed by lung computed tomography in normal subjects and patients with chronic obstructive pulmonary disease. *Proc Natl Acad Sci USA* 96: 8829–8834, 1999.
23. **Murakami S, Nagaya N, Itoh T, Iwase T, Fujisato T, Nishioka K, Hamada K, Kangawa K, and Kimura H.** Adrenomedullin regenerates alveoli and vasculature in elastase-induced pulmonary emphysema in mice. *Am J Respir Crit Care Med* 172: 581–589, 2005. First published June 9, 2005; 10.1164/rccm.200409–1280OC.
24. **Nakano Y, Muro S, Sakai H, Hirai T, Chin K, Tsukino M, Nishimura K, Itoh H, Pare PD, Hogg JC, and Mishima M.** Computed tomographic measurements of airway dimensions and emphysema in smokers. Correlation with lung function. *Am J Respir Crit Care Med* 162: 1102–1108, 2000.
25. **Oldmixon EH, Butler JP, and Hoppin FG.** Semi-automated measurement of true chord length distributions and moments by video microscopy and image analysis. *J Microsc* 175: 60–69, 1994.
26. **Otsu N.** A threshold selection method from gray-level histograms. *IEEE Trans Sys Man Cybernetics* 9: 62–66, 1979.
27. **Robbesom AAVE, Veerkamp JH, van Krieken JH, Bulten HJ, Smits HT, Willems LN, van Herwaarden CL, Dekhuijzen PN, and van Kuppevelt TH.** Morphological quantification of emphysema in small human lung specimens: comparison of methods and relation with clinical data. *Mod Pathol* 16: 1–7, 2003.
28. **Roerdink JBTM and Meijster A.** The watershed transform: definitions, algorithms and parallelization techniques. *Fundamenta Informaticae* 41: 187–228, 1999.
29. **Rubio ML, Martin-Mosquero MC, Ortega M, Peces-Barba G, and Gonzalez-Mangado N.** Oral *N*-acetylcysteine attenuates elastase-induced pulmonary emphysema in rats. *Chest* 125: 1500–1506, 2004.
30. **Russi EW, Bloch KE, and Weder W.** Functional and morphological heterogeneity of emphysema and its implication for selection of patients for lung volume reduction surgery. *Eur Respir J* 14: 230–236, 1999.
31. **Saetta M, Shiner RJ, Angus GE, Kim WD, Wang NS, King M, Ghezzo H, and Cosio MG.** Destructive index: a measurement of lung parenchymal destruction in smokers. *Am Rev Respir Dis* 131: 764–769, 1985.
32. **Santalo LA.** *Integral Geometry, and Geometric Probability.* Reading, MA: Addison-Wesley, 1976, p. 217–220.
33. **Snider G, Kleinerman J, Thurlbeck W, and Bengali Z.** The definition of emphysema: report of a national heart, lung and blood institute, division of lung diseases workshop. *Am Rev Respir Dis* 132: 182–185, 1985.
34. **Soutiere SE, Tankersley CG, and Mitzner W.** Differences in alveolar size in inbred mouse strains. *Respir Physiol Neurobiol* 140: 283–291, 2004.
35. **Suki B, Lutchen KR, and Ingenito EP.** On the progressive nature of emphysema: roles of proteases, inflammation, and mechanical forces. *Am J Respir Crit Care Med* 168: 516–521, 2003.
36. **Tang K, Rossiter HB, Wagner PD, and Breen EC.** Lung-targeted VEGF inactivation leads to an emphysema phenotype in mice. *J Appl Physiol* 97: 1559–1566, 2004.
37. **Thurlbeck W.** Internal surface area and other measurements in emphysema. *Thorax* 22: 483–496, 1967.
38. **Tomkeieff SI.** Linear intercepts, areas and volumes. *Nature* 155: 24, 1945.
39. **Weibel ER and Gomez DM.** Principle for counting tissue structures on random sections. *J Appl Physiol* 17: 343–348, 1962.
40. **Weibel ER and Gomez DM.** Architecture of the human lung. *Science* 137: 577–585, 1962.
41. **Wong AKC and Sahoo PK.** A gray-level-threshold selection method based on maximum entropy principle. *IEEE Trans Sys Man Cybernetics* 19: 866–871, 1989.